Modeling of Spray-Formed Materials: Geometrical Considerations

Y.J. LIN, J.E. BOBROW, D.R. WHITE, and E.J. LAVERNIA

In this article, a mathematical model is formulated to predict the evolution and final geometry of an axisymmetric billet (*i.e.*, round) obtained using an off-axis spray arrangement. The model is formulated by calculating the shape change of a profile curve of a billet surface, based on an axisymmetric surface. On the basis of this model, a methodology to determine the "shadowing effect" coefficient is presented. The modeling results suggest that there are three distinct regions in a spray-formed billet: a base transition region, a uniform diameter region, and an upper transition region. The effects of several important processing parameters, such as the withdrawal velocity of substrate, maximum deposition rate, spray distribution coefficient, initial eccentric distance, and rotational velocity of substrate, on the shape factors (*e.g.*, the diameter size of the uniform region and the geometry of the transition regions) are investigated. The mechanisms responsible for the formation of the three distinct regions are discussed. Finally, the model is then implemented and a methodology is formulated to establish optimal processing parameters during spray forming, paying particular attention to deposition efficiency.

I. INTRODUCTION

SPRAY forming is a manufacturing technique in which partially solidified metal droplets are dispersed upon a substrate to produce an almost fully dense material in tonnage quantities. Available studies show that the thermal and solidification conditions that are present during spray forming promote several desirable characteristics, such as microstructural refinement,[1,2,4,5] extended solubility,[1,4] and, in some cases, the appearance of nonequilibrium phases.[1] For the production of near-net-shape deposits, the droplet size and spatial distribution are of interest because the deposit shape resembles the spatial distribution of droplet mass arriving at the deposition surface. The droplet size and spatial distribution are related to the type of atomizer used and to operating variables. In the atomization of metals, circular gas jet nozzles represent a type of atomizer that is commonly used. Therefore, there exists a limitation in that the droplet mass distribution exhibits a Gaussian distribution centered about the spray axis. To that effect, specific experimental arrangements have been taken to approach a variety of geometries, including rings, billets, tubes, and cylinders, while using circular atomizers.

Experimental and simulation efforts have been conducted on the geometry of plates[7–11] and tubes.[12] However, three-dimensional growth during buildup of round billets leads to complexities in the required control protocols, as a result of transient phenomena that develop under certain conditions. One example of such transient phenomena is described in the literature as a shadowing effect,[14] which leads to the formation of columnar porosity.[6] Exploring the optimal processing parameters through experimentation is time-consuming and not economical. Hence, computer simulation is a useful approach to investigating the formation and development of round billets.[15] Several mathematical models have been developed to calculate the growth of round billets.[13–22] These models aim at the selection of optimal processing parameters, the design of spray-forming chambers and plants, and the investigation of the thermal transfer.

In related studies, Frigaard *et al.* formulated a mathematical model to investigate the growth dynamics of spray-formed billets.[14,19–21] In their model, a partial differential equation describing the average motion of a billet's surface is formulated. Numerical solution of the partial differential equation is then implemented to study both transient billet growth and steady-state crown shapes of spray-formed aluminum billets, and the atomizer scanner angle function for a perfect shape billet is computed.

Mathur *et al.*,[17] Muhamad *et al.*[18], and Elgobashi *et al.* [25] have independently established their models to predict the buildup of round billets. They divided the substrate surface into many grid points. Using a scanning spray mode, they obtain the shape of billets by accumulating the height growth in all grid points. Considering the fact that, in practice, sticking efficiency is less than 100 pct, Mathur *et al.*[24] incorporate sticking efficiency into shape calculation, in order for shape modeling to reflect the real situation.

More recently, Seok *et al.*[15,16] formulated a three-dimensional model to predict the motion dynamics of a billet's surface. In their formulation, the surface is obtained by determining the position of all points at any instant. Moreover, Seok *et al.* use computer graphics to illustrate the shadowing effect. They demonstrate that in the case of a static, vertical atomizer the spray axis must be inclined relative to the rotation axis in order to obtain the desired billet morphology. Additionally, Kang *et al.*[22] used the method to update the points in the current billet's surface into the new points to calculate the evolution of a billet using a scanning gas atomizer.

An off-axis, confined atomization device is advantageous

Y.J. LIN, Graduate Student, and E.J. LAVERNIA, Professor, Department of Chemical and Biochemical Engineering and Materials Science, and J.E. BOBROW, Professor, Department of Mechanical and Aerospace Engineering, are with the University of California Irvine, Irvine, CA 92697-2575. D.R. WHITE, Principal Engineering Specialist, is with the Materials Systems Reliability Department, Ford Research Laboratory, Dearborn, MI 48121-2053.

Manuscript submitted August 2, 1999.

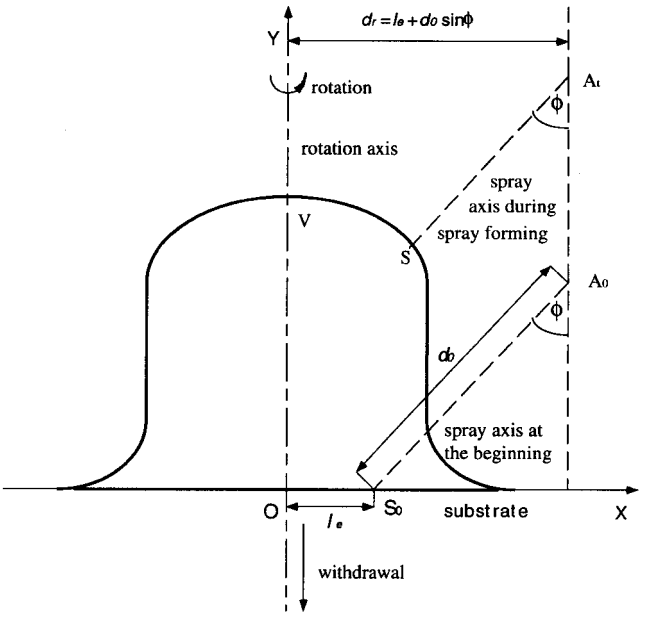

Fig. 1—Schematic diagram illustrating the spray mode used in the present study.

from the standpoint of atomization efficiency. Inspection of the available literature, however, reveals that fundamental information on billet geometry using this type of spray mode is limited. Consequently, the objective of the present article is to formulate a mathematical model to predict the evolution and final geometry of an axisymmetric billet. The mathematical formulation is described as follows. First, formulas are developed to calculate the growth of any point in the surface of an axisymmetric billet. Second, the new shape of each profile curve on the surface, *i.e.*, the generatrix of an axisymmetric billet, is defined by the new positions of all points in the profile curve. The assembly of all profile curves in their new positions comprises the new surface of an axisymmetric billet. On the basis of the numerical simulation results, the effects of several important processing parameters on the surface morphology of round billets are analyzed. The mechanisms that are responsible for the formation of three distinct regions and two types of base transition regions of axisymmetric billets are investigated in detail and optimal processing parameters are deduced.

II. DESCRIPTION OF SPRAY-FORMING MODE

The spatial distribution of atomized mass flux generated by a circular atomizer is generally described using a Gaussian function; consequently, the atomizer and/or substrate must be displaced to overcome inherent geometrical constraints.[1] The spray mode refers to the movements of the atomizer and the substrate and the relative positions between them. In this article, the following spray-forming mode is employed, as described in Figure 1.

(1) During spray forming, the substrate rotates at a uniform angular velocity ω and withdraws at a uniform velocity v. The rotation center of the substrate is O. The vertex V of a spray-formed round billet is defined as the intersection point between its instant surface and the rotation axis of the substrate.

(2) During spray forming, the atomizer is maintained at a fixed spatial location. The spray axis, *i.e.*, the axis of the atomizer, is located in the plane determined by the diameter of the substrate and the rotation axis of the substrate. The spray axis is inclined to the rotation axis of the substrate at an angle ϕ, termed the spray angle. There exists a distance $d_r = l_e + d_0 \sin \phi$ between the atomizer and the spray axis, which is unchanged, as shown in Figure 1. At the beginning of spray forming, the atomizer is at the position A_0. At this moment, the spray axis intersects the substrate plane at the point S_0. The distance between the point O and S_0 is defined as the initial eccentric distance l_e. The distance between the point A_0 and S_0 is d_0.

III. MATHEMATICAL FORMULATION

Spray forming comprises the steps of spray atomization and deposition. In the spray-atomization step, molten metal/alloy is disintegrated into a spray of droplets by gas atomization. Then, the droplets are initially accelerated and then decelerated by the atomization gas as it moves toward a substrate.[1,3] The droplets are deflected by the aerodynamic interactions that take place between the droplets and the atomization gas in the vicinity of the spray-formed billet.[23] In the present model formulation, it is assumed that droplets travel from the atomizer to the deposition point along a straight line.

In the deposition step, only a definite fraction of the droplets impinging on the substrate or of previously deposited droplets is incorporated into the surface of the spray-formed material (*i.e.*, billet).[23,24] Some of the droplets fail to adhere to the surface as a result of either bounce-off phenomena or flow-field effects. The proportion of droplets that comprise the spray-formed material may be defined using a sticking efficiency (SE). The SE is determined by two factors: the angle of incidence between the direction of droplet motion and the surface normal, and the solid fraction.[24] Consequently, it is evident that the final morphology of an axisymmetric billet is influenced, not only by the thermal and momentum fields of the impinging droplet array, but also by the surface characteristics of the billet.[24,28] The interaction between shape evolution and solidification renders the analysis complex. In the present formulation, the SE is assumed to be unity, in order to simplify the problem formulation.

A. *Evolution of Surface Profile*

In a plane perpendicular to the spray axis, the distribution of mass rate *vs* the distance away from the spray axis may be expressed as a Gaussian function.[1–3,16,18,25–27] On the basis of the assumption, the deposition rate per unit areas in a generic point P in the surface of a billet is given from the following formula (Appendix):

$$\dot{H} = \left| \frac{\mathbf{e_n} \cdot \mathbf{e_f}}{\mathbf{e_s} \cdot \mathbf{e_f}} \right| \cdot \xi \cdot a \cdot \exp(-b \cdot s^2) \qquad [1]$$

where $\dot{H}$ ($mm^3/mm^2 \cdot s$) is the deposition rate per unit areas; a ($mm^3/mm^2 \cdot s$) and b (mm^{-2}) are the maximum deposition rate and the spray distribution coefficient, respectively; s is the shortest distance between a point and the spray axis; $\mathbf{e_n}$

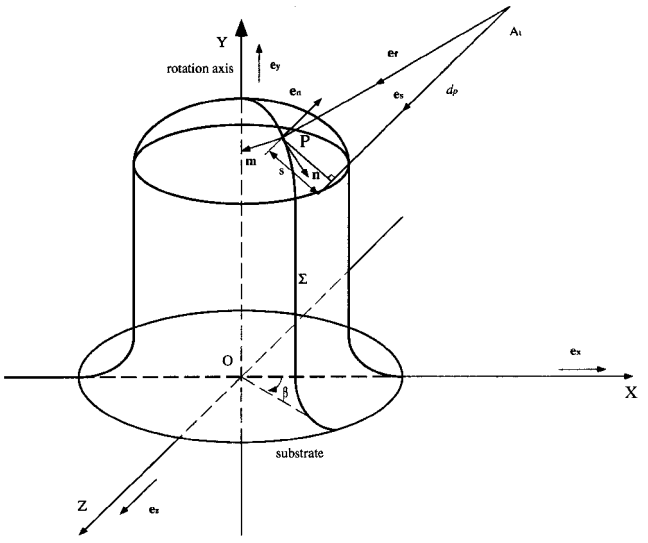

Fig. 2—Generation of a profile curve of billet surface and its evolution in the Cartesian coordinate system during spray forming.

is the unit normal vector in point P; $\mathbf{e_s}$ is a unit vector in the direction of the spray axis, and $\mathbf{e_f}$ is a unit vector in the flight direction of droplets. The maximum deposition rate a and the spray distribution coefficient b vary with the distance d_p between the atomizer and the plane perpendicular to the spray axis and passing through point P, according to the following equation:[16]

$$\frac{a_s}{a} = \frac{b_s}{b} = \left(\frac{d_p}{d_s}\right)^2 \qquad [2]$$

where a_s (mm^3/mm^2·s) and b_s (mm^{-2}) are the maximum deposition rate and the spray distribution coefficient at the reference distance d_s between the atomizer and the plane perpendicular to the spray axis, respectively. The term ξ is the shadowing effect coefficient ($\xi = 1$ or 0) that is discussed in the following section.

The deposited height Δh in the direction normal to the surface ($\mathbf{e_n}$ in Figure 2) during a short interval from t to $t + \Delta t$ can be calculated from the following formula:

$$\Delta h = \int_t^{t+\Delta t} \left|\frac{\mathbf{e_n} \cdot \mathbf{e_f}}{\mathbf{e_s} \cdot \mathbf{e_f}}\right| \cdot \xi \cdot a \cdot \exp(-b \cdot s^2)\, dt \qquad [3]$$

Assuming that the position vectors of the present point P and the new point P^n are $\mathbf{p}$ and $\mathbf{p}^n$, respectively, then

$$\mathbf{p^n} = \mathbf{p} + \Delta h \cdot \mathbf{e} \qquad [4]$$

As shown in Figure 2, a Cartesian coordinate system is established according to the following methodology: (1) choose the rotation center of the substrate O as the origin; (2) choose the rotation axis of the substrate as the y-axis; and (3) choose the two radial directions perpendicular to each other as the x-axis and z-axis such that the atomizer is located in the XOY plane ($X > 0$). For convenience purposes, assume that the atomizer moves upward at the withdrawal velocity of the substrate ν.

On the basis of the preceding formulation, a straight line that starts at the rotation center O, along any radius, and the rotation axis of the substrate determine a unique plane. The plane intersects with the billet surface to produce a profile curve Σ, as shown in Figure 2. An assembly of all profile curves constitutes the surface of a round billet. Evolution of any profile curve Σ is analyzed as follows: At a certain moment, the angle between the XOY plane, the plane determined by the profile curve Σ, and the rotation axis is β. The position vectors of the atomizer A_t and any point P in the surface are $\mathbf{a_t}$ and $\mathbf{p}$, respectively. From point P, one makes a plane perpendicular to the spray axis. The distance between the atomizer and the plane is d_p. The shortest distance between the deposited point P and the spray axis is s, and the unit vector of the droplet flight direction is $\mathbf{e_f}$. They are given by the following equations:[16]

$$d_p = \mathbf{e_s} \cdot (\mathbf{p} - \mathbf{a_t}) \qquad [5]$$

$$s = \|\mathbf{a_t} + d_p \cdot \mathbf{e_s} - \mathbf{p}\| \qquad [6]$$

$$\mathbf{e_f} = \frac{\mathbf{p} - \mathbf{a_t}}{\|\mathbf{p} - \mathbf{a_t}\|} \qquad [7]$$

A high angular velocity of substrate rotation ω leads to an axisymmetric surface of revolution.[15,16] In the case of a round billet, an axisymmetric profile is desirable. The profile curve Σ is called the generatrix[29] for the surface of revolution, which represents the billet surface. Thus, the normal direction of the surface at point P is identical to that of the profile curve Σ at point P and in the plane determined by the profile curve and y-axis. Suppose that $\mathbf{n}$ is the tangential line of the profile curve, as shown in Figure 2. The position vector of point P', another point very near P in the profile curve, is $\mathbf{p}'$. Then, $\mathbf{n}$ is approximated by the vector ($\mathbf{p}'$-$\mathbf{p}$). Assuming that $\mathbf{m}$ is the normal vector of the plane determined by the profile curve Σ and y-axis, the unit normal vector of the profile curve Σ at point P and in the plane determined by the profile curve Σ and y-axis, *i.e.*, the unit normal vector $\mathbf{e_n}$ of surface at point P, is given from the following equation:

$$\mathbf{e_n} = \frac{\mathbf{m} \times \mathbf{n}}{\|\mathbf{m} \times \mathbf{n}\|} \qquad [8]$$

If one divides the time of a rotation into a number of very short time intervals Δt, then the growth and new coordinates of any point P can be calculated from Eqs. [1] through [8]. The new positions of all points in the profile curve determine its new geometry. Subsequently, the profile curve rotates to a new position, $\beta + \Delta\beta$. The preceding calculation procedure is then repeated.

Rigorously, the preceding treatment is correct only upon the completion of k rotations (k is a positive integer). However, a high rotational velocity of substrate ω and therefore a short deposition time during a rotation can be selected for an axisymmetric profile shape. Hence, within a single rotation, the shape difference between the profile curves can be safely neglected.

In order to obtain axisymmetric billets, a reasonable value of ω is first determined. A low rotational velocity of substrate ω leads to an asymmetric surface.[15,16] Large errors will appear when the evolution of a profile curve Σ is calculated according to the preceding method of determining $\mathbf{e_n}$. Meanwhile, when the preceding methodology is used to evaluate $\mathbf{e_n}$, the calculated surface based on such $\mathbf{e_n}$ is asymmetric. Figures 3(a) and (b) show the calculated profile curves at angular velocities of substrate rotation, 15 deg/s and 90 deg/s,

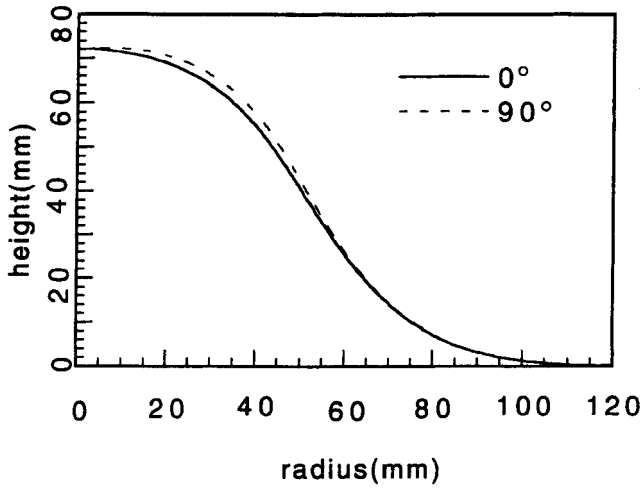

(*a*)

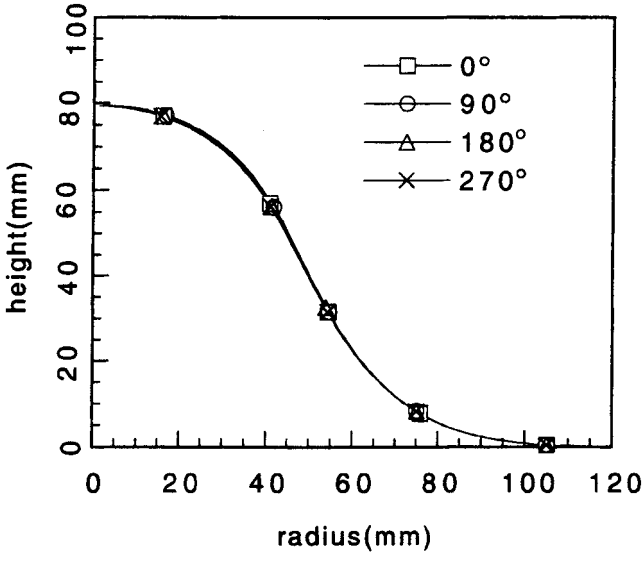

(*b*)

Fig. 3—Calculated profile curves at different rotational velocities: (*a*) $\omega = 15$ deg/s and (*b*) $\omega = 90$ deg/s. Other processing parameters: $a_s = 2.5$ mm/s, $b_s = 0.0015$ mm^{-2}, $\nu = 0.8$ mm/s, $l_e = 50$ mm, $d_0 = 500$ mm, $\phi = 35$ deg, and $\Delta t = 144$ s.

respectively. Figure 3(a) shows the two profile curves with initial angles of 0 and 90 deg, respectively, after 144 seconds of deposition time (at the beginning of spray forming, the angle between the *XOY* plane ($X > 0$) and the plane determined by the profile curve and the *y*-axis is called the initial angle). The two profile curves fail to coincide after 144 seconds of deposition time. This result implies that the surface is asymmetric at a rotational velocity of 15 deg/s. In Figure 3(b), the four profile curves with initial angles 0, 90, 180, and 270 deg appear to coincide after 144 seconds of deposition time, suggesting that the surface is axisymmetric for a rotational velocity of 90 deg/s. In the discussion that follows, it is assumed that an axisymmetric surface is desirable, as far as the ultimate billet geometry is concerned. Moreover, the surface of a billet is described by using a profile curve of the billet.

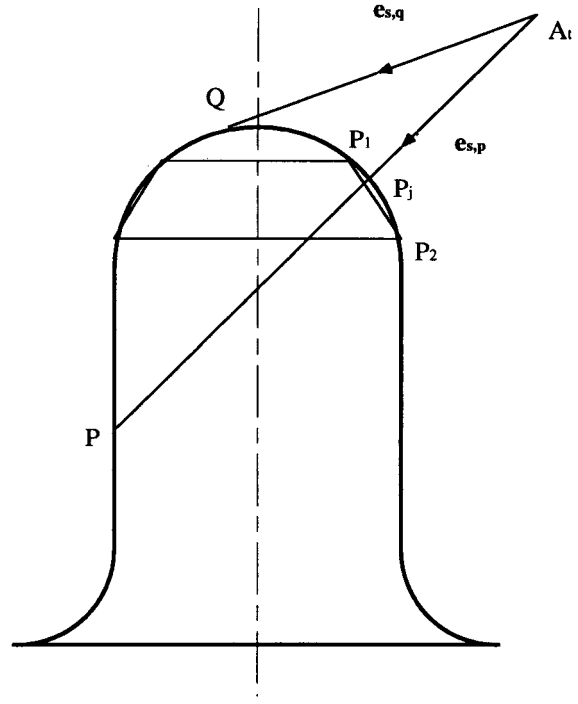

Fig. 4—Schematic diagram used to illustrate the determination of the shadowing effect coefficient.

B. *Shadowing Effect*

The atomized droplets travel from the atomization point to the target along a straight line. Hence, a deposition will attain its target location (*i.e.*, trajectory A_t-Q in Figure 4), as long as it does not encounter a physical obstacle (*i.e.*, trajectory A_t-P in Figure 4). If one defines ξ as a shadowing effect coefficient, then $\xi = 1$ when droplets can reach a specific point (*i.e.*, Q), whereas $\xi = 0$ when droplets are unable to reach that particular point (*i.e.*, P).

Without analytical equations for any profile curve, it is divided into a number of curve sections. Any curve section approximates a straight-line segment when it is sufficiently small (*i.e.*, in Figure 4, curve section P_1P_2 is regarded as straight-line segment P_1P_2). The entire billet surface can be approximately considered to consist of surfaces of revolution of all these straight-line segments about the rotation axis. Let the coordinates of P_1 and P_2 be (x_1, y_1, z_1) and (x_2, y_2, z_2), respectively. Then, the equation describing the surface of revolution determined by the straight-line segment P_1P_2 about the rotation axis of substrate is as follows:[29]

$$x^2 + z^2 = \left[\frac{(y - y_1)\left(\sqrt{x_2^2 + z_2^2} - \sqrt{x_1^2 + z_1^2}\right)}{y_2 - y_1} + \sqrt{x_1^2 + z_1^2} \right]^2, \quad y_1 \le y \le y_2 \qquad [9]$$

The straight-line equation defining a path between the atomizer $A_t(d_r, y_a, 0)$ and the point $P(x_p, y_p, z_p)$ being deposited is as follows:

$$\frac{x - d_r}{x_p - d_r} = \frac{y - y_a}{y_p - y_a} = \frac{z}{z_p} \qquad [10]$$

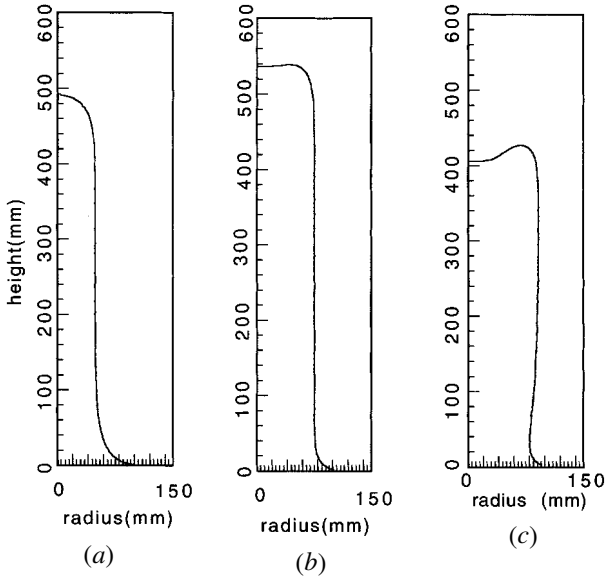

Fig. 5—Calculated surfaces of round billets with different withdrawal velocities of substrate: (*a*) $\nu = 2.6$ mm/s, $\Delta t = 200$ s; (*b*) $\nu = 1.2$ mm/s, $\Delta t = 450$ s; and (*c*) $\nu = 0.8$ mm/s, $\Delta t = 500$ s. Other processing parameters: $a_s = 10$ mm/s, $b_s = 0.0015$ mm^{-2}, $l_e = 50$ mm, $d_0 = 500$ mm, $\omega = 720$ deg/s, $\phi = 35$ deg.

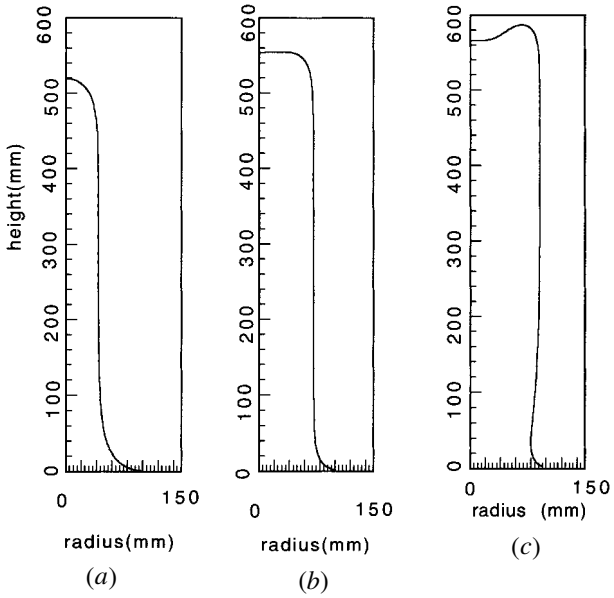

Fig. 6—Calculated surfaces of round billets with different maximum deposition rates: (*a*) $a_s = 2.5$ mm/s, (*b*) $a_s = 6$ mm/s, and (*c*) $a_s = 10$ mm/s. Other processing parameters: $b_s = 0.0015$ mm^{-2}, $\nu = 0.8$ mm/s, $l_e = 50$ mm, $d_0 = 500$ mm, $\phi = 35$ deg, $\omega = 720$ °/s, and $\Delta t = 700$ s.

The coordinates of the intersection points between the surface of revolution formed by the straight-line segment P_1P_2 about the rotation axis and the straight line connecting the atomizer A_t and the point P are the solution to Eqs. [9] and [10]. The existence of a solution means that the straight line A_tP intersects the surface of revolution. Otherwise, they do not intersect. In Figure 4, at any point P on the billet's surface, if at least one of the intersection points between the straight line A_tP and these surfaces of revolution formed by the straight-line segment joining two neighboring points about the rotation axis is located between the atomizer A_t and point P, the point P is shadowed by the billet's surface ($\xi = 0$): it will be unable to grow. Otherwise, $\xi = 1$ and it will grow.

IV. NUMERICAL RESULTS

Figures 5(a) through (c) are the calculated surfaces of billets for the following withdrawal velocities: $\nu = 0.8$, 1.2, and 2.6 mm/s. All of the calculated surfaces contain three distinct regions: a base transition region, a uniform diameter region, and an upper transition region. The diameter and deposition efficiency in the uniform diameter region increase with decreasing withdrawal velocity ν. Calculated diameters with $\nu = 0.8$, 1.2, and 2.6 are approximately 182, 148, and 97 mm, respectively, whereas the deposition efficiency in the uniform diameter stage is about 99, 98, and 92 pct, respectively.

There exist two types of base transition regions. The first type is illustrated in Figures 5(a) and (b). In a two-dimensional profile curve of billets, with increasing height, the side-surface angle of the billet increases until it reaches 90 deg. The portion of the billet below this point is called a type I base transition region. The second type is illustrated in Figure 5(c). Similar to the case shown in Figures 5(a) and (b), in a profile curve, the angle of the side surface increases with increasing height until a value of 90 deg is reached. Unlike that shown in Figures 5(a) and (b), however, the side-surface angle continues to increase until the side surface is inclined outward. At a certain height, the surface angle reaches 90 deg again. The portion of the billet below this second point is defined hereafter as a type II base transition region. The geometry of the base transition regions changes from type I to type II with decreasing withdrawal velocities from $\nu = 2.6$ mm/s to 0.8 mm/s.

The top geometry of the upper transition regions changes from convex to concave with decreasing ν from 2.6 to 0.8 mm/s. Actually, depending on the relative position of the plane passing through the vertex V and perpendicular to the rotation axis, an upper transition region is divided into two parts: a lower portion and a top portion. In the case of flat and convex transition regions, the length of the top portion is considered as zero. With $\nu = 2.6$, 1.2, and 0.8 mm/s, the length of the top portion is approximately 0, 4, and 20 mm, respectively, whereas the length of the lower portion is approximately 70, 45, and 17 mm, respectively. Accordingly, with a decrease in withdrawal velocity ν, the length of the top portion increases and the length of the lower portion decreases.

Figures 6 through 9 show the effects of the maximum deposition rate a_s, the spray distribution coefficient b_s (constant a_s/b_s), the initial eccentric distance l_e, and the rotational velocity of the substrate ω, respectively, on the surface morphology of the billets, which are summarized in Table I.

V. DISCUSSION

A. *Growth Dynamics of Round Billets*

On the basis of the present model formulation, the growth rate at any point during rotation mainly depends on the

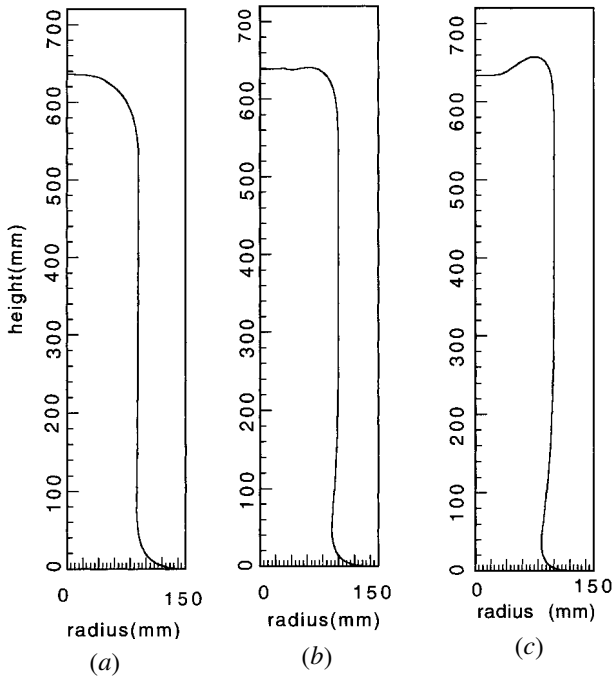

Fig. 7—Calculated surfaces of round billets with different spray distribution coefficients: (*a*) $b_s = 0.0004$ mm^{-2}, (*b*) $b_s = 0.0008$ mm^{-2}, and (*c*) $b_s = 0.0012$ mm^{-2}. Other processing parameters: $a_s/b_s = 12{,}500$ mm^3/s, $\nu = 1.24$ mm/s, $l_e = 50$ mm, $d_0 = 500$ mm, $\phi = 35$ deg, $\omega = 720$ deg/s, $\Delta t = 500$ s.

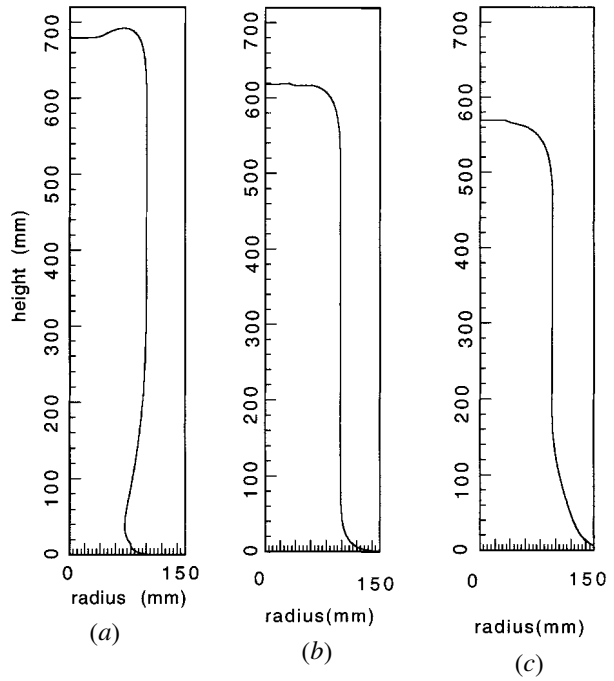

Fig. 8—Calculated surfaces of round billets with different initial eccentric distances: (*a*) $l_e = 20$ mm, (*b*) $l_e = 65$ mm, and (*c*) $l_e = 100$ mm. Other processing parameters: $a_s = 10$ mm/s, $b_s = 0.0008$ mm^{-2}, $\nu = 1.24$ mm/s, $d_0 = 500$ mm, $\phi = 35$ deg, $\omega = 720$ deg/s, $\Delta t = 500$ s.

distance s between the point and the spray axis (Figure 2). Points on the profile curve with large values of s have smaller growth rates. Consider the growth of a profile curve during

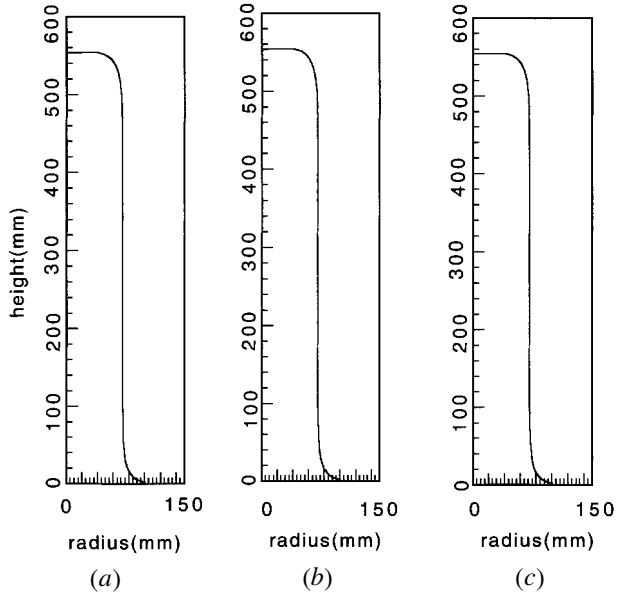

Fig. 9—Calculated surfaces of round billets with different rotational velocities of substrate: (*a*) $\omega = 360$ deg/s, (*b*) $\omega = 720$ deg/s, and (*c*) $\omega = 1080$ deg/s. Other processing parameters: $a_s = 6$ mm/s, b_s, $= 0.0015$ mm^{-2}, $\nu = 0.8$ mm/s, $l_e = 50$ mm, $d_0 = 500$ mm, $\phi = 35$ deg, and $\Delta t = 700$ s.

a single rotation. For the profile curve shown in Figures 10(a) and (c), the intersection point between the spray axis and the profile curve is T. On one hand, for those points beyond point T on the profile curve, the distance s to the spray axis increases with increasing the radius r no matter where the profile curve has revolved to during a single rotation. On the other hand, as shown in Figures 10(a) and (c), any two points B_1 and B_2 (with corresponding radii $r_1 < r_2$) located between the vertex V and point T are sometimes closer to the spray axis (with $s_1 < s_2$) and sometimes farther from the spray axis (with $s_1 > s_2$) depending on the location of the profile curve as it revolves around the spray axis. As a result, a remarkable height difference between two neighboring points beyond the point T occurs and the surface angle increases rapidly compared with any two points between V and T. For this reason, the surface beyond T is defined hereafter as the "side surface," whereas the surface between T and V is termed the "top surface." With the buildup of the billet, the surface angles of the side surface will become greater and greater until the value of 90 deg is reached at a certain point. For example, under spray-forming parameters in Figures 5(a) and (c), the times before the surface angles start to become 90 deg are about 103 and 90 seconds, respectively, as shown in Figures 10(a) and (c). After this moment, the billets continue to grow in two different growth modes: therefore, two different types of base transition regions will develop. The effect of the withdrawal velocity of substrate ν is taken as an example to explain how the two different types of base transition regions form.

High withdrawal velocity of substrate always leads to type I base transition regions, as shown in Figure 10(a). In a profile curve, when the value of 90 deg is reached at a certain point C, the high withdrawal velocity of substrate results in a large distance between point C and the spray axis. The distance s between the point and the spray axis is approximately 80 mm in XOY plane ($X > 0$), as shown in

Table I. The Effects of Several Important Processing Parameters on Base and Upper Transition Regions

Processing Parameters	ν Increase	l_e Increase	a_s Decrease	b_s Decrease	ω Increase
Base transition region	type II to type I	type II to type I	type II to type I	type II to type I	unchanged
Upper transition region	concave to convex	concave to convex	concave to convex	concave to convex	unchanged
Top portion of upper transition region	length decrease	length decrease	length decrease	length decrease	unchanged
Lower portion of upper transition region	length increase	length increase	length increase	length increase	unchanged
Remarks				constant a_s/b_s	

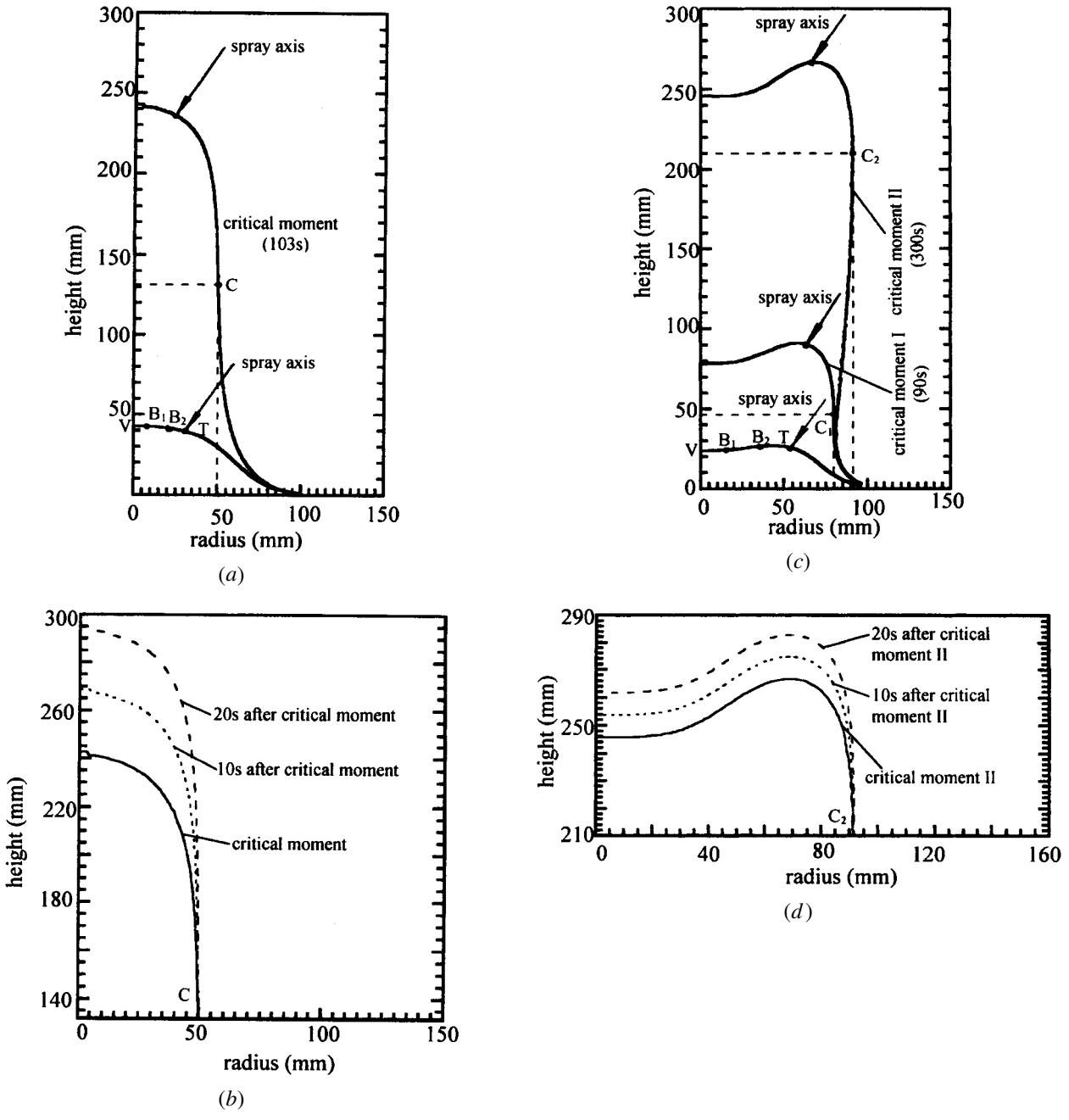

Fig. 10—Mechanism for the two types of base transition region. (*a*) Mechanism for type I base transition region. (*b*) Stable growth in the first growth mode. (*c*) Mechanism for type II base transition region. (*d*) Stable growth in the second growth mode.

Figure 10(a). The distance is so large that the deposited mass in the point is negligible; therefore, almost no height growth occurs in the point. Thus, the surface angle will stay at 90 deg. Furthermore, this growth mode involves stable growth

immediately after the moment called the critical moment. As shown in Figure 10(b), the surface points above point C move with the same vertical velocity. Accordingly, after that moment, the side surface will remain vertical until the spray-forming experiment is completed. In this way, a region with uniform diameter is formed. The section of the billet below point C at the critical moment is called a type I base transition region. The section of the billet above point C at the critical moment is the upper transition region of the final billet, as mentioned in Section IV. However, if the withdrawal velocity of the substrate is too large, the value of 90 deg of surface angle cannot be attained before the spray axis reaches the vertex V. Thus, billets with constant diameters cannot be spray-formed. The critical withdrawal velocity of the substrate is given from the following equation:[15]

$$\nu_{\text{cri}} = a_s \cos \phi \left(\frac{d_s \sin \phi}{l_e + d_0 \sin \phi} \right)^2 \qquad [11]$$

Type II base transition regions arise under a low withdrawal velocity of substrate. At the moment (called the critical moment I) the value of 90 deg is reached at a point C_1 in the profile curve (Figure 10(c)), the distance between the spray axis and the point is not large due to the low withdrawal velocity of the substrate and the short time to reach the critical moment I. The distance s between the point and the spray axis is approximately 35 mm in the XOY plane ($X > 0$) (Figure 10(c)). It enables growth at the point. The radial growth at the point continues to increase the surface angle to more than 90 deg and the side surface is inclined outward. Meanwhile, the radial growth increases the distance between the spray axis and the point of 90 deg of surface angle. Accordingly, the value of the surface angles inclined outward is gradually reduced. Finally, at a moment called the critical moment II, the distance between the spray axis and the point of 90 deg of surface angle (point C_2) is so large (the distance between point C_2 and the spray axis in the XOY plane ($X > 0$) is approximately 55 mm) that almost no height growth occurs in the point. The subsequent growth is similar to the stable growth in the first growth mode (Figure 10(d)). The section of the billet below point C_2 at the critical moment II is called a type II base transition region. The section of the billet above point C_2 at the critical moment II is the upper transition region of the final billet, as noted in Section IV.

The effects of the other important processing parameters, such as l_e, a_s, b_s, and ω, on the shape of the base transition region are summarized in Table I. It appears that at the start of spray forming, the factors that lead to an increase in height growth rate also promote the formation of type II base transition regions, because they bring about a shorter time to reach the value of 90 deg of side surface and therefore a smaller distance between the spray axis and the point with 90 deg of surface angle.

The characteristics of the upper transition region result from the cumulative growth effect of top surface before stable growth is reached. Due to the undetermined relationship of the r and s of any two points in the part of the top surface of a profile curve, as well as to the change of relative position between the spray axis and the rotation axis, the formation of the upper transition region is complex. The effects of several important processing parameters on the upper transition region are listed in Table I.

It is interesting that, in the stage of stable growth that occurs after the critical moment in Figure 10(a) for a type I base transition region and after the critical moment II for a type II base transition region, the top surface moves at the same velocity as the withdrawal velocity of substrate. Actually, after the start of spray forming, the relative positions between the spray axis and points on the billet's surface continuously change due to different vertical movement velocity until these velocities become equal to each other. The vertex is taken as an example to explain the preceding change. During spray forming, when the withdrawal velocity of the substrate is higher than that of the vertex growth, the distance between the spray axis and the vertex decreases. This results in an increase of the vertex growth. In this way, the differential velocity diminishes continuously and eventually approaches zero. Afterward, the growth velocity of the vertex and the relative position between the spray axis and the vertex will remain unchanged. When the withdrawal velocity of the substrate is lower than that of the vertex growth, the distance between the spray axis and the vertex increases; therefore, the vertex growth decreases. Finally, the difference between the values of the two velocities almost reaches zero. Figures 11(a) and (b) show the velocity change of the vertex with different withdrawal velocities of substrate and with different initial eccentric distances, respectively. It is observed that the vertex velocity eventually approaches the withdrawal velocity of the substrate independent of the processing parameters that are used. Once the withdrawal velocity of the substrate becomes equal to the growth velocity of the vertex, the relative position between the spray axis and the vertex remains constant. Similarly, the relative position between the spray axis and other points in the top surface remains constant at different moments. At the critical moment for the first type of growth mode (Figure 10(a)) and the critical moment II for the second type of growth mode (Figure 10(c)), the relative positions between the spray axis and all points in the top surface remain constant.

The diameter D of the uniform region can be calculated from the following equation:[16]

$$D = 2 \sqrt{\frac{\overline{Ya_s}}{b_s \nu}} \qquad [12]$$

where Y is the deposition efficiency in the uniform diameter stage, a parameter that is related to geometric factors associated with round billets. Equation [12] is applicable only if the actual withdrawal velocity of substrate is below the critical one obtained from Eq. [11]. According to calculated results, the effects of several important processing parameters on Y are summarized in Table II. Thus, according to Eq. [12], the D changes with several important processing parameters can be as shown in Table II.

B. *Optimal Processing Parameters*

Spray forming is of interest not only from the standpoint of metallurgical characteristics (*i.e.*, refined microstructure and phase metastability) but also as a result of the potential for near net-shape fabrication. There are two critical issues that currently hinder widespread application of this technology: porosity and material yield. The issue of porosity is currently the topic of intense numerical[35,36,37] and experimental[33,34,38] investigations. The loss of material is attributed to[23] (a) droplets that fail to collect during deposition

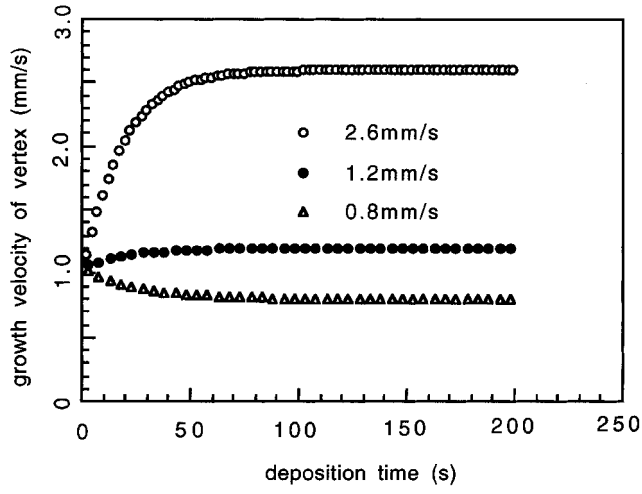

(*a*)

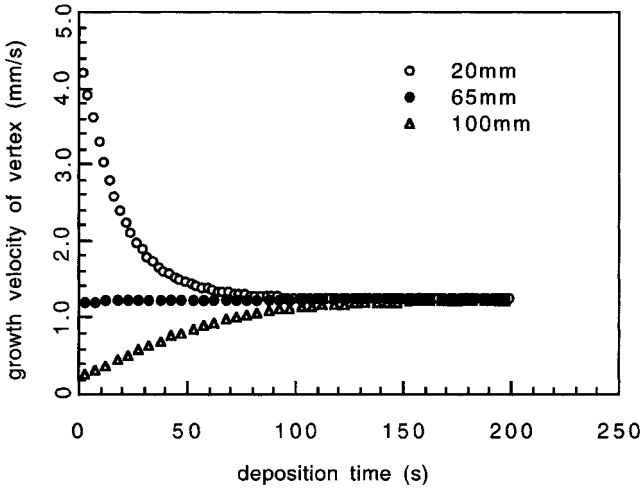

(*b*)

Fig. 11—The change of growth velocity of the vertex with different (*a*) withdrawal velocity and (*b*) initial eccentric distance. Processing parameters in (a): a_s = 10 mm/s, b_s = 0.0015 mm^{-2}, l_e = 50 mm, d_0 = 500 mm, ω = 720 deg/s, and ϕ = 35 deg. Processing parameters in (b): a_s = 10 mm/s, b_s = 0.0008 mm^{-2}, ν = 1.24 mm/s, d_0 = 500 mm, ω = 720 deg/s, and ϕ = 35 deg.

(overspray powders) as a result of surface effects (*i.e.*, deposition efficiency); (b) droplets that bounce off from the deposition surface; (c) scalping or machining in order to attain the required diameter; and (d) machining or trimming of the base and upper transition regions. A reduction of the total material losses implies low production costs; therefore, it is beneficial to the commercialization of spray-forming technology.

In the present model formulation, we assumed a sticking efficiency of 100 pct; accordingly, material losses due to bounce-off (b) are neglected. Hence, the optimal processing parameters are those that minimize the total loss of material attributable to (a), (c), and (d) earlier, while maintaining the required diameter.

Material losses due to (a) are related to deposition efficiency, the ratio of mass deposited in the substrate to the total atomized one. According to the preceding calculation results, dynamic growth of spray-formed round billets consists of two stages: a transition growth stage and a stable growth stage. In regular production, the time of the stable growth stage accounts for a larger proportion of time than that of the transition growth stage. Thus, a high deposition efficiency during the stable growth stage, *e.g.*, in excess of 99 pct is one of the criteria used to determine the optimal processing parameters.

In industrial production, the objective is typically to produce round billets with a required diameter. Assuming that the required round billet is D_p in diameter and R_p in radius, then

$$\frac{Ya_s}{b_s\nu} = R_p^2 \qquad [13]$$

where $Y \geq 99$ pct. If Y is taken as 99 pct, the actual diameter of the uniform area, R, is slightly higher than R_p when the actual deposition efficiency is more than 99 pct. However, a small amount of machining will reduce them into the required radius, and material losses in (c) are minimized. Thus, a deposition yield of 99 pct is selected as a basis to establish optimal processing parameters. Accordingly, Eq. [13] is changed into

$$\frac{0.99a_s}{b_s\nu} = R_p^2 \qquad [14]$$

Equation [14] defines the necessary condition for optimal processing parameters. First of all, of course, the optimal processing parameters must satisfy the critical condition for spray-formed round billets denoted by Eq. [11]. In addition, the rotational velocity of substrate ω must be high enough to produce an axisymmetric profile.

Spray-formed round billets are usually hot-extruded to achieve full density and to improve mechanical properties; this requires a uniform diameter. Thus, the upper transition regions must be trimmed.[2,18] Type I transition regions need to be machined into a desired diameter, whereas type II transition regions must be trimmed. The sum of the trimmed and machined volumes of the base and upper transition regions, called the removal volume, comprises material losses in (d). Hence, the total value of the removal volume must be minimized for optimal processing.

In general, the optimal processing parameters are characterized by the following features: (1) the diameter is equal

Table II. The Effects of Several Important Processing Parameters on Deposition Efficiency and Diameter in Stable Growth Stage

Processing Parameters	ν Increase	l_s Increase	a_s Decrease	b_s Decrease	ω Increase
Deposition efficiency	decrease	decrease	decrease	decrease	unchanged
Diameter	decrease	decrease	decrease	decrease	unchanged
Remark	—	—	—	constant a_s/b_s	—

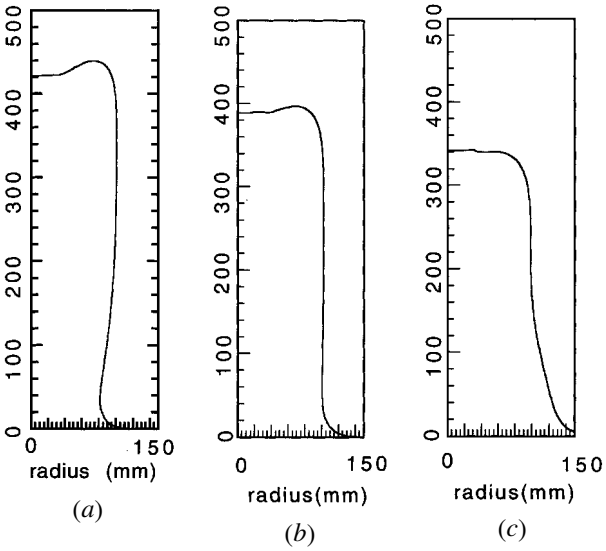

Fig. 12—Calculated surfaces of round billets with different initial eccentric distance: (*a*) l_e = 40 mm, (*b*) l_e = 65 mm, and (*c*) l_e = 100 mm. Other processing parameters: a_s = 10 mm/s, b_s = 0.0010 mm^{-2}, ν = 0.98 mm/s, d_0 = 500 mm, ϕ = 35 deg, ω = 720 deg/s, and Δt = 400 s.

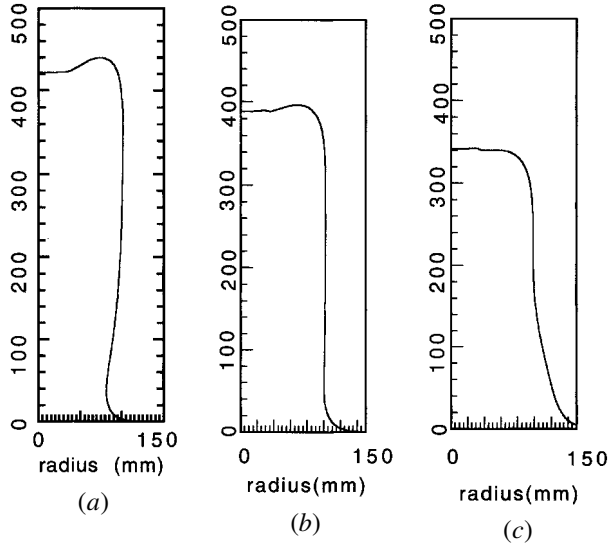

Fig. 13—Calculated surfaces of round billets with different initial eccentric distance: (*a*) l_e = 40 mm, (*b*) l_e = 65 mm, and (*c*) l_e = 100 mm. Other processing parameters: a_s = 4 mm/s, b_s = 0.001 mm^{-2},ν = 0.392 mm/s, d_0 = 500 mm, ϕ = 35 deg, ω = 720 deg/s, and Δt = 1000 s.

to or slightly higher than the target one, (2) the deposition efficiency during stable growth stage exceeds 99 pct, and (3) the removal volume is maintained at a minimum value.

A specific example is taken to describe a methodology to explore optimal processing parameters. In this example, a round billet of diameter D = 200 mm is to be spray-formed with a fixed d_0 = 500 mm, ϕ = 35 deg, and ω = 720 deg/s. Assuming that the spray distribution coefficient b_s is available in the range of 0.0004 to 0.0015 mm^{-2}, a series of spray distribution coefficients b_s = 0.0004, 0.0008, 0.0010, 0.0012, and 0.0015 mm^{-2} are selected. For any value of the b_s, each surface is calculated with a different a_s (ν is determined by b_s and a_s from Eq. [14]) and l_e. For example,
b_s = 0.0010 mm^{-2}, and Figures 12 and 13 show the calculated surface with a_s = 10 mm/s and a_s = 4 mm/s, respectively. It is worth noting that the two calculated surfaces with the same l_e in Figures 12 and 13 possess the same diameter of uniform region, and the same shape of base and upper transition regions. This results from the fact that the opposite effects of a_s and ν on the diameter of the uniform region and on the shape of upper and base transition regions, as discussed in the preceding paragraphs, counteract each other. Thus, the same b_s (therefore a_s/ν) and l_e result in the same shape characteristics, independent of a_s. Thus, for every b_s, there exists an optimal l_e, in which the minimum removal volume will be obtained. Comparing these minimum removal volumes at the different b_s, optimal processing parameters can be determined.

On the basis of the critical condition, as defined by Eq. [11], the range of l_e, which enables round billets to be spray-formed, is determined. The maximum l_{em} can be calculated from the following formula:

$$l_{em} = d_s \cdot \sin\phi \cdot \left(\sqrt{\frac{a_s \cos\phi}{\nu}} - \frac{d_0}{d_s} \right) \qquad [15]$$

where l_{em} are 133, 303, 376, 436, and 525 mm, corresponding to b_s = 0.0004, 0.0008, 0.0010, 0.0012, and 0.0015 mm^{-2}, respectively.

For each value of b_s =0.0004, 0.0008, 0.0010, 0.0012, and 0.0015 mm^{-2}, a series of surface and removal volumes are calculated at different l_e. With b_s = 0.0004 mm^{-2} and a very small initial eccentric distance l_e = 1 mm, the diameter of the uniform region is about 190 mm, as shown in Figure 14(a). In this case, round billets of 200 mm in diameter cannot be produced, because the diameter of uniform region decreases with an increase of initial eccentric distance l_e (1 mm is approximately considered as minimum initial eccentric distance). Figures 14(b) through (e) show the calculated surfaces with minimum removal volume, as well as the required diameter of uniform region, with b_s = 0.0008, 0.0010, 0.0012, and 0.0015 mm^{-2}. Their removal volumes are 8.34 × 10^6, 1.34 × 10^6, 1.19 × 10^6, and 0.90 × 10^6 mm^3. With the diameter of uniform region about 200 mm, the long type II base transition region and upper transition region of the calculated billet at b_s = 0.0008 mm^{-2} lead to a greater trimmed volume than those corresponding to b_s = 0.0010, 0.0012, and 0.0015 mm^{-2}. The calculated round billets for b_s = 0.0010, 0.0012, and 0.0015 mm^{-2} possess almost the same type I base transition region. With an increase in b_s, the length of the lower part of these concave upper transition regions decreases, whereas the length of the upper part increases. In the range of b_s = 0.0010 to 0.0015 mm^{-2}, because the decrease of trimmed volume resulting from the decrease of the length of the lower part is dominant, the total removal volume decreases. Thus, the processing parameters in Figure 14(e), b_s = 0.0015 mm^{-2}, a_s/ν = 15.3, l_e = 77 mm, d_0 = 500 mm, ϕ = 35 deg, and ω = 720 deg/s, represent those required for optimal deposition conditions.

It should be noted that in the case of practical industrial production, several factors need to be taken into consideration. The first consideration is the maximum dimensions of the spray-forming chamber. Obviously, the horizontal dimensions of the chamber limit the maximum distance between the atomizer and the spray axis, $d_r = l_e + d_0 \sin\phi$. The second consideration is that the spray distribution

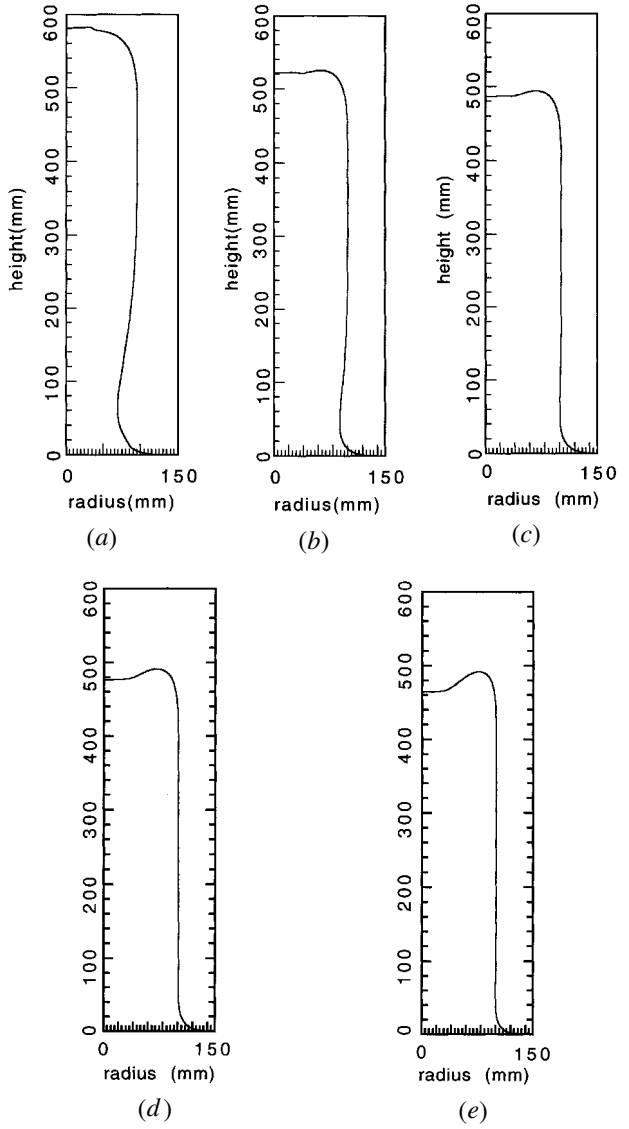

Fig. 14—Calculated surfaces of round billets with minimum removal volume at different b_s: (*a*) $b_s = 0.0004\ \text{mm}^{-2}$, $a_s = 10$ mm/s, $l_e = 1$ mm, and $\Delta t = 200$ s; (*b*) $b_s = 0.0008\ \text{mm}^{-2}$, $a_s = 10$ mm/s, $l_e = 45$ mm, and $\Delta t = 400$ s; (*c*) $b_s = 0.0010\ \text{mm}^{-2}$, $a_s = 10$ mm/s, $l_e = 68$ mm, and $\Delta t = 500$ s; (*d*) $b_s = 0.0012\ \text{mm}^{-2}$, $a_s = 10$ mm/s, $l_e = 72$ mm, and $\Delta t = 600$ s; and (*e*) $b_s = 0.0015\ \text{mm}^{-2}$, $a_s = 15$ mm/s, $l_e = 77$ mm, and $\Delta t = 500$ s. Other processing parameters: a_s/b_s ν = 10,101 mm^2, $\omega = 720$ deg/s, $d_0 = 500$ mm, and $\phi = 35$ deg.

coefficient b_s cannot be selected arbitrarily: b_s is mainly determined by the specific atomizer design. Besides b_s, atomization efficiency and subambient aspiration base pressure at the tip of the delivery tube also need to be considered when the atomizer is designed.[30,31,32] The third consideration arises from the demand to reduce porosity in billets. A large eccentric distance, l_e, and d_0 will likely result in a long flight distance and, therefore, porous billets.[33,35] The fourth consideration is related to the flow rate of molten alloys. As indicated in the above paragraph, a_s/ν is an item of optimal processing parameters. The simultaneous increase of a_s (the increase of the flow rate of molten alloy) and ν favor the improvement of productivity per unit of time. However, an increase in the flow rate of the molten alloy should be accompanied by a corresponding increase in the flow rate of the atomization gas in order to obtain the desired size and distribution of droplets.[1] The increase is always restricted by the design of the atomizers, because many other factors, such as the value of b_s and the subambient aspiration base pressure, as previously mentioned in the second consideration, must be considered.

VI. CONCLUSIONS

1. A mathematical model has been established to analyze the shape change of a profile curve of an axisymmetric surface corresponding to a round billet during spray forming. In this case, the shape of the profile curve represents the entire morphology of the surface. By using the model, the surface of round billets produced under various processing parameters has been calculated.
2. In the case of a tilting spray and a fixed atomizer, a spray-formed round billet consists of three regions: a base transition region, a uniform diameter region, and an upper transition region.
3. There are several important processing parameters that influence the morphology of round billets and the diameters of the stable growth stage. These results are summarized in Tables I and II.
4. On the basis of the maximum deposition efficiency during the stable growth stage and the minimum removal volume, to obtain billets with uniform diameters, a methodology to explore the optimal processing parameters is formulated. Those combinations of processing parameters with the same a_s/ν and other parameters (*i.e.*, b_s, l_e, ϕ, and ω) lead to the almost same geometry of billets, although a_s and ν are different. Processing parameters $b_s = 0.0015\ \text{mm}^{-2}$, $a_s/\nu = 15.3$, and $l_e = 77$ mm represent optimal processing parameters when a round billet of diameter $D = 200$ mm is spray-formed with $b_s = 0.0004$ to $0.0015\ \text{mm}^{-2}$, $d_0 = 500$ mm, $\phi = 35$ deg, and $\omega = 720$ deg/s.

APPENDIX
Calculation of growth in a general point

The unit normal vector of the very small area dA_n is $\mathbf{e_n}$, as shown in Figure 15. Connect all points in the boundary of the area with the atomizer A to form a cone. In area dA_n, make one plane perpendicular to the spray axis and the other one perpendicular to the straight line between the atomizer and the area dA_n. The two planes intersect with the side surface of the preceding cone to produce areas dA_s and dA_f, respectively. Due to the very small area dA, those lines connecting the boundary of the area dA_n with the atomizer are almost parallel.

$$dA_f = dA_s \cdot |\mathbf{e_s} \cdot \mathbf{e_f}| \quad [16]$$

$$dA_f = dA_n \cdot |\mathbf{e_n} \cdot \mathbf{e_f}| \quad [17]$$

It then follows that

$$dA_s = \left|\frac{\mathbf{e_n} \cdot \mathbf{e_f}}{\mathbf{e_s} \cdot \mathbf{e_f}}\right| \cdot dA_n \quad [18]$$

The deposition rate through the area dA_s is calculated from the following equation:

$$\dot{M} = a \cdot \exp(-b \cdot s^2)\, dA_s \quad [19]$$

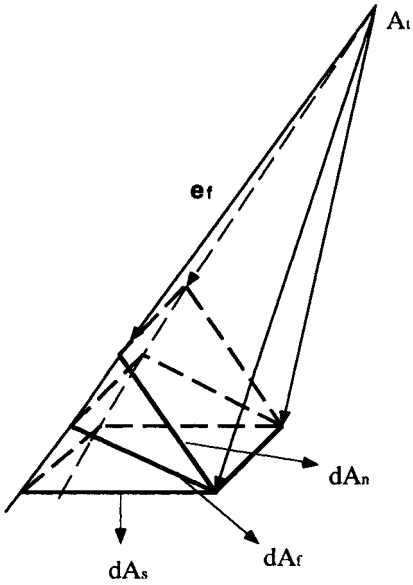

Fig. 15—Schematic diagram for growth calculation in unit area with unit normal vector $\mathbf{e_n}$.

Because the mass flux passing through the three areas, dA, dA_s, and dA_f, is the same, the deposition rate per unit area in dA_n (incorporating shadow effect coefficient ξ) is

$$\dot{H} = \left|\frac{\mathbf{e_n} \cdot \mathbf{e_f}}{\mathbf{e_s} \cdot \mathbf{e_f}}\right| \cdot \xi \cdot a \cdot \exp(-b \cdot s^2) \qquad [1]$$

NOMENCLATURE

$\dot{H}$	deposition rate per unit area ($mm^3/mm^2 \cdot s$)
Δh	normal growth distance of a point during a time interval (mm)
Δt	deposition time interval (s)
d_s	reference distance, *i.e.*, distance between the atomizer and a reference plane perpendicular to the spray axis (mm)
d_p	distance between the atomizer and any plane perpendicular to the spray axis (mm)
d_r	the distance between the atomizer and the rotation axis (mm)
a_s	maximum deposition rate at reference distance (mm/s)
b_s	spray distribution coefficient at reference distance (mm^{-2})
a	maximum deposition rate (mm/s)
b	spray distribution coefficient (mm^{-2})
s	the shortest distance between a deposited point and the spray axis (mm)
ξ	shadowing effect coefficient
x_p, y_p, z_p	Cartesian coordinates of a point P in billet surface
$x_1\ y_1, z_1$ and x_2, y_2, z_2	Cartesian coordinates of any two neighboring points in a profile curve
$\mathbf{a_t}$	position vector of the atomizer
$\mathbf{p}$	position vectors of point P in billet surface
$\mathbf{p}'$	position vector of a point P′ very near P in the element curve
$\mathbf{e_n}$	unit normal vector of a point P
$\mathbf{e_s}$	unit vector of spray axis
$\mathbf{e_f}$	unit vector of flight direction from the atomizer to a point P
$\mathbf{n}$	tangential vector of a point P
$\mathbf{m}$	normal vector of a plane determined by *Y*-axis and a profile curve
$\|\mathbf{V}\|$	Euclidean norm of a vector $\mathbf{V}$
β	angle between the positive direction of X-axis and the plane determined by a profile curve and Y-axis (°)
ω	rotational velocity of substrate (°/s)
ν	withdrawal velocity of substrate (mm/s)
ν_{cri}	critical withdrawal velocity of substrate to spray form round billets (mm/s)
l_e	initial eccentric distance of the spray axis (mm)
l_{em}	maximum initial eccentric distance to spray form billets (mm)
ϕ	inclined angle of the spray axis to the rotation axis (°)
Y	deposition efficiency in stable growth stage
D	diameter of uniform region (mm)
R_p	required billet diameter in industrial production (mm)
O	the center of substrate
V	vertex of a round billet
T	intersection point between the spray axis and the profile curve in XOY plane ($X > 0$)
A_0	initial position of the atomizer
A_t	atomizer position during spray forming
S_0	intersection point between the initial spray axis and the substrate
S	intersection point between the spray axis and billet surface at any moment
P, Q, P_1, P_2, P_j, P^n	points in billet surface
Σ	a profile curve

ACKNOWLEDGMENT

The authors acknowledge the financial support from the United States Department of Energy (DE-FC07-00ID13816).

REFERENCES

1. E.J. Lavernia and Y. Wu: *Spray Atomization and Deposition*, John Wiley & Sons, Inc., New York, NY, 1996.
2. P.S. Grant: *Progr. Mater. Sci.*, 1995, vol. 39, pp. 497-545.
3. P. Mathur, D. Apelian, and A. Lawley: *Acta Metall.*, 1989, vol. 37, pp. 429-43.
4. P.S. Grant, W.T. Kim, B.P. Bewlay, and B. Cantor: *Scripta Metall.*, 1989, vol. 23, pp. 1651-56.
5. A.G. Leatham and A. Lawley: *Int. J. Powder Metall.*, 1993, vol. 29, p. 321.
6. Z.H. Lee, H. Hu, E.J. Lavernia, and D.R. White: *Metall. Mater. Trans. A*, 2000, vol. 31A, pp. 723-33.
7. G. Hartmann, P.N. Hansen, and P.R. Sahm: *Modeling and Control of Casting and Welding Processes IV*, TMS, Warrendale, PA, 1988, pp. 915-21.
8. B.W. Oh and Z.H. Lee: *Proceeding of Modeling of Casting and Solidification Process*, Yonsei University, Seoul, Korea, 1991, pp. 13-22.
9. S. Annavarapu, D. Apelian, and A. Lawley: *Metall. Trans. A*, 1990, vol. 21A, pp. 3237-56.
10. C.Y. Tsao and N.J. Grant: *Int. J. Powder Metall.*, 1994, vol. 30, pp. 323-33.
11. Men G. Chu: *Proc. 3rd Int. Conf. on Spray Forming*, Wales, United Kingdom, Osprey Metals Ltd., Neath, West Glamorgan, 1997, pp. 27-35.

12. R. Rebis, C. Madden, T. Zappia, and C. Cai: *Proc. 3rd Int. Conf. on Spray Forming*, Wales, United Kingdom, Osprey Metals Ltd., Neath, West Glamorgan, 1996, pp. 281-85.
13. A.G. Leatham: *Proc. 2nd Int. Conf. on Spray Forming*, Swansea, United Kingdom, Osprey Metals Ltd., Neath, West Glamorgan, 1994, pp. 129-40.
14. I.A. Frigaard: *SIAM J. Appl. Math.*, 1995, vol. 55, pp. 1161-1203.
15. H.K. Seok, D.H. Yeo, K.H. Oh, H.Y. Ra, D.S. Shin, and H.I. Lee: *Proc. 3rd Int. Conf. on Spray Forming*, Wales, United Kingdom, 1996, pp. 287-95.
16. H.K. Seok, D.H. Yeo, K.H. Oh., H.I. Lee, and H.Y. Ra: *Metall. Mater. Trans. B*, 1998, vol. 29B, pp. 699-708.
17. P. Mathur, D. Apelian, and A. Lawley: *Powder Metall.*, 1991, vol. 34, p. 109.
18. N. Muhamad, J.O. Medwell, and D.T. Gethin: *Powder Metall.*, 1995, vol. 38, pp. 214-20.
19. I.A. Frigaard and O. Scherzer: *SIAM J. Appl. Math.*, 1997, vol. 57, pp. 649-82.
20. I.A. Frigaard: *J. Mater. Proc. Manuf. Sci.*, 1994, vol. 3, pp. 173-92.
21. I.A. Frigaard: *J. Mater. Proc. Manuf. Sci.*, 1995, vol. 3, pp. 257-75.
22. S. Kang, D.H. Chang, E.S. Lee, and S. Ahn: *Mater. Sci. Eng. A*, vol. 260A, 1999, pp. 161-69.
23. C. Kramer, V. Uhlenwinkel, and K. Bauckhage: *Proc. 3rd Int. Conf. on Spray Forming*, Wales, United Kingdom, 1996, pp. 273-80.
24. P. Mathur, S. Annavarapu, D. Apelian, and A. Lawley: *Mater. Sci. Eng. A*, vol. 142A, 1991, pp. 261-76.
25. S. Elgobashi, T. Abu-arab, M. Rizk, and A. Mostafa: *Int. J. Multiphase Flow*, 1984, vol. 10, pp. 697-710.
26. C.-Y.A. Tsao and N.J. Grant: *Powder Metall. Int.*, 1994, vol. 30, pp. 323-33.
27. U. Fritsching, H. Zhang, and K. Bauckhage: *Steel Res.*, 1994, vol. 65, p. 273.
28. Q. Xu, V.V. Gupta, and E.J. Lavernia: *Metall. Mater. Trans. B*, 1999, vol. 30B, pp. 527-39.
29. D.M.Y. Sommerville: *Analytical Geometry of Three Dimensions*, The Syndics of Cambridge University Press, London, 1959.
30. Aderson, R.S. Figliola, and H. Morton: *Mater. Sci. Eng. A*, 1991, vol. 148A, p. 101.
31. J.C. Baram, M.K. Veistinen, E.J. Lavernia, M. Abinante, and N.J. Grant: *J. Mater. Sci.*, 1988, vol. 23, p. 2457.
32. M.K. Veistinen, E.J. Lavernia, M. Abinante, and N.J. Grant: *Mater. Lett.*, 1987, vol. 5, p. 373.
33. S. Annavarapu, D. Apelian, and A. Lawley: *Metall. Trans. A*, 1988, vol. 19A, pp. 3077-86.
34. W.D. Cai, J. Smugeresky, and E.J. Lavernia: *Mater. Sci. Eng. A*, 1998, vol. 241, pp. 60-71.
35. W.D. Cai and E.J. Lavernia: *Metall. Mater. Trans. B*, 1998, vol. 29B, pp. 1085-96.
36. W.D. Cai and E.J. Lavernia: *Metall. Mater. Trans. B*, 1998, vol. 29B, pp. 1097-1106.
37. W.D. Cai and E.J. Lavernia: *Mater. Sci. Eng. A*, 1997, vols. 226–228, pp. 8-12.
38. S. Annavarapu and R. Doherty: *Int. J. Powder Metall.*, 1993, vol. 29, pp. 331-43.